Biallelic loss-of-function variations in PRDX3 cause cerebellar ataxia

Adriana Rebelo, Ilse Eidhof, Vivian Cintra, Léna Guillot-Noel, Claudia Pereira, Dagmar Timmann, Andreas Traschütz, Ludger Schöls, Giulia Coarelli, Alexandra Durr, et al.

Biallelic loss-of-function variations in PRDX3 cause cerebellar ataxia

Adriana P. Rebelo,[1] Ilse Eidhof,[2] Vivian P. Cintra,[1] Léna Guillot-Noel,[3,4] Claudia V. Pereira,[5] Dagmar Timmann,[6] Andreas Traschütz,[7,8] Ludger Schöls,[7,8] Giulia Coarelli,[3] Alexandra Durr,[3,9] Mathieu Anheim,[10,11] Christine Tranchant,[10,11] Bart van de Warrenburg,[12] Claire Guissart,[13] Michel Koenig,[13] Jack Howell,[1] Carlos T. Moraes,[5] Annette Schenck,[2] Giovanni Stevanin,[3,4] Stephan Züchner[1,2] and Matthis Synofzik[7,8,2] on behalf of the PREPARE network

[†]These authors contributed equally to this work.

Peroxiredoxin 3 (PRDX3) belongs to a superfamily of peroxidases that function as protective antioxidant enzymes. Among the six isoforms (PRDX1–PRDX6), PRDX3 is the only protein exclusively localized to the mitochondria, which are the main source of reactive oxygen species. Excessive levels of reactive oxygen species are harmful to cells, inducing mitochondrial dysfunction, DNA damage, lipid and protein oxidation and ultimately apoptosis. Neuronal cell damage induced by oxidative stress has been associated with numerous neurodegenerative disorders including Alzheimer's and Parkinson's diseases.

Leveraging the large aggregation of genomic ataxia datasets from the PREPARE (Preparing for Therapies in Autosomal Recessive Ataxias) network, we identified recessive mutations in *PRDX3* as the genetic cause of cerebellar ataxia in five unrelated families, providing further evidence for oxidative stress in the pathogenesis of neurodegeneration. The clinical presentation of individuals with *PRDX3* mutations consists of mild-to-moderate progressive cerebellar ataxia with concomitant hyper- and hypokinetic movement disorders, severe early-onset cerebellar atrophy, and in part olivary and brainstem degeneration. Patient fibroblasts showed a lack of PRDX3 protein, resulting in decreased glutathione peroxidase activity and decreased mitochondrial maximal respiratory capacity. Moreover, *PRDX3* knockdown in cerebellar medulloblastoma cells resulted in significantly decreased cell viability, increased H_2O_2 levels and increased susceptibility to apoptosis triggered by reactive oxygen species. Pan-neuronal and pan-glial *in vivo* models of *Drosophila* revealed aberrant locomotor phenotypes and reduced survival times upon exposure to oxidative stress.

Our findings reveal a central role for mitochondria and the implication of oxidative stress in *PRDX3* disease pathogenesis and cerebellar vulnerability and suggest targets for future therapeutic approaches.

1 Dr. John T. Macdonald Foundation Department of Human Genetics and John P. Hussman Institute for Human Genomics, University of Miami Miller School of Medicine, Miami, USA
2 Department of Human Genetics, Donders Institute for Brain, Cognition, and Behavior, Radboud University Medical Centre, Nijmegen, The Netherlands
3 Sorbonne Université, Paris Brain Institute, AP-HP, INSERM, CNRS, Pitié-Salpêtrière University Hospital, Paris, France
4 Neurogenetics Team, EPHE, PSL University, Paris, France
5 Departments of Neurology and Cell Biology, University of Miami Miller School of Medicine, Miami, FL, USA
6 Department of Neurology, Essen University Hospital, University of Duisburg-Essen, Essen, Germany

7 Translational Genomics of Neurodegenerative Diseases, Hertie-Institute for Clinical Brain Research, University of Tübingen, Tübingen, Germany
8 German Center for Neurodegenerative Diseases (DZNE), University of Tübingen, Tübingen, Germany
9 Department of genetics, Hôpital de La Pitié-Salpétrière, Paris, France
10 Département de Neurologie, Hôpital de Hautepierre, Hôpitaux Universitaires de Strasbourg, Strasbourg, France
11 Institute of Genetics and Molecular and Cellular Biology, INSERM-U964/CNRS-UMR7104, University of Strasbourg, Illkirch, France
12 Department of Neurology, Radboud University Medical Centre, Donders Institute for Brain, Cognition and Behaviour, Nijmegen, The Netherlands
13 EA7402 Institut Universitaire de Recherche Clinique and Laboratoire de Génétique Moléculaire, CHU and Université de Montpellier, Montpellier, France

Correspondence to: Stephan Züchner, MD, PhD
Department of Human Genetics
University of Miami Miller School of Medicine
Biomedical Research Building (BRB)
Room 616, LC: M-860
1501 NW 10th Avenue
Miami, FL 33136, USA
E-mail: szuchner@med.miami.edu

Correspondence may also be addressed to: Prof. Dr. Matthis Synofzik
Translational Genomics of Neurodegenerative Diseases, Hertie Institute for Clinical Brain Research
University of Tübingen
Hoppe-Seyler-Str. 3, 72076 Tübingen, Germany
E-mail: matthis.synofzik@uni-tuebingen.de

Keywords: PRDX3; ROS; ataxia

Abbreviation: SARA = Scale for the Assessment and Rating of Ataxia

Introduction

Hereditary cerebellar ataxias are a heterogeneous group of neurodegenerative diseases resulting from progressive damage to the cerebellum and/or its associated afferent tracts,[1–3] which occur with a prevalence of ~26/100 000 around the globe.[4] Although more than 200 genes have been associated with different types of ataxia, many patients remain undiagnosed, in particular if presenting as a simplex case. Among the key hubs underlying hereditary ataxia, dysfunction of mitochondrial pathways has emerged as a common theme, uniting in particular a multitude of autosomal-recessive ataxias and thus highlighting a shared, potentially targetable cluster of pathways underlying cerebellar vulnerability.[3,5] Several autosomal-recessive ataxias either directly affect nuclear-encoded mitochondrial proteins (e.g. Friedreich's ataxia or ataxias related to POLG, TWNK, ADCK3/COQ8A, SPG7 and ATAD3A) or are indirectly linked to mitochondria metabolism (e.g. autosomal recessive spastic ataxia of Charlevoix-Saguenay).[3] As the most common autosomal-recessive ataxia, Friedreich's ataxia results from reduced expression of the mitochondrial protein frataxin.[6] Evidence suggests that reduced frataxin leads to the accumulation of iron in mitochondria, which promotes Fenton-mediated oxidative stress, indicating mitochondrial dysfunction and oxidative stress as a mechanism of the disease.[7] High levels of reactive oxygen species can lead to both nuclear and mitochondrial DNA damage, lipid peroxidation, protein oxidation and apoptosis. Antioxidants have been shown to improve cardiac and skeletal muscle bioenergetics in patients with Friedreich's ataxia, suggesting oxidative stress as a central pathological role.[8]

Mutations in the mitochondrial DNA polymerase gamma (*POLG*) can cause cerebellar ataxia as a result of neuronal loss in the olivary-cerebellum area.[9–11] Multiple mitochondrial DNA deletions are observed in patients with *POLG* mutations, which are considered to be the main mechanism of the disease. Likewise, cerebellar ataxia is also a highly frequent clinical phenotype in patients with other mitochondrial diseases, which are not primarily subsumed to autosomal-recessive ataxias.[12,13] Although several lines of evidence thus indicate that cerebellar ataxia can be caused by mitochondrial defects, the underlying mechanisms remain to be elucidated. Despite many studies suggesting increased oxidative stress and mitochondrial DNA damage,[14] other conflicting reports do not support that mechanism. In this study, we present *PRDX3*, which encodes a mitochondrial antioxidant protein, as a recurrent cerebellar ataxia gene, linking for the first time mutant *PRDX3* to a human disease. *PRDX3* encodes peroxiredoxin 3, a member of the peroxiredoxin family which catalyses the reduction of hydrogen peroxide (H_2O_2), playing a major role against oxidative stress.[15] PRDX3 functions as a dodecamer complex ring composed of 12 assembled subunits of PRDX3 molecules.[16] Upon reaction with H_2O_2, its cysteine is oxidized, forming an intermolecular disulphide bond with the cysteine from another subunit. This intermolecular disulphide bond is reduced back by thioredoxin (TXN2) and the redox cycle is reinitiated.[17] Interestingly, a loss-of-function mutation in *TXN2* causes early onset neurodegeneration with severe cerebellar atrophy, epilepsy, dystonia and peripheral neuropathy.[18] The use of antioxidant pharmacological compounds such as idebenone was shown to improve TNX2 loss-of-function symptoms in a single individual. However, a larger number of patients would be necessary to better evaluate the effects of the drug. Downregulation of *PRDX3* in cells has also been shown to have detrimental consequences affecting mitochondrial mass, morphology and membrane potential.[19] Here, we report five simplex families with biallelic mutations in *PRDX3* leading to complete loss of its encoded protein. Our molecular studies with patient fibroblasts, cerebellar medulloblastoma cells

and *Drosophila* indicate oxidative stress and mitochondrial dysfunction to be the underlying disease mechanism. Our study provides novel insights into the regulatory pathways of PRDX-mediated H_2O_2 detoxification, and the consequences of its absence on the cellular and organismal level.

Materials and methods

Patient in-depth phenotyping

Patients were recruited via the international network 'Preparing for therapies in autosomal-recessive ataxias' (PREPARE; https://www.prepare-ataxia.com). In-depth phenotyping was performed in all patients by neurologists who were ataxia specialists, including standardized assessments of ataxia and non-ataxia symptoms, nerve conduction studies, EMG and 1.5- or 3-T cerebral MRI investigations. Disease severity was assessed clinically by the Scale for the Assessment and Rating of Ataxia (SARA)[20] and functional impairment by the Spinocerebellar Degeneration Functional Score (SDFS).[21] All patients gave written consent to participate in the study. The study protocol was approved by the institutional review board of the University of Tübingen (Az 598/2011BO1) as well as the other local institutional review boards.

Whole-exome and sanger sequencing

Whole-exome sequencing was performed in the five index individuals. The SureSelect Human All Exon Kit (Agilent) was used for in-solution enrichment, and the HiSeq 2500 instrument (Illumina) was used to produce 100 bp paired-end sequence reads. The Burrows-Wheeler aligner was used for sequence alignment and Freebayes was used for variant calling. Whole-exome sequencing data were uploaded into the GENESIS platform and analysed as part of the >1700 whole-exome sequencing ataxia datasets compiled by the PREPARE ataxia consortium (www.prepare-ataxia.com) within GENESIS.[22] Variants were validated by Sanger Sequencing (Eurofins) and sequencing traces were analysed using the Sequencher software (GeneCodes).

Structural modelling

A structural model of the PRDX3 dodecamer ring complex was built using Yasara software (Elmar Krieger). The crystal structure of the human PRDX3 protein was used as a template (PDBID 5UCX). A ribbon diagram was created to visualize the folding and secondary structures of protein. The patients' missense mutations were mapped to their corresponding positions.

Cell culture

Fibroblasts cells were obtained from five affected individuals (Probands 1–5) and four healthy control individuals (including an unaffected heterozygous sister of Proband 1) by skin biopsy. Cells were cultured in low glucose (1 g/l) Dulbecco's modified Eagle medium (Thermo Fisher Scientific) supplemented with sodium pyruvate and 10% foetal bovine serum (FBS). Daoy cells from a cerebellar medulloblastoma (ATCC) were cultured on Eagle's minimum essential medium with 10% FBS. Cells were incubated at 37°C in 5% CO_2.

Immunofluorescence

Cells were seeded and grown on covered chamber slides. The next day, the cells were washed with PBS and fixed with 4% paraformaldehyde (PFA) for 15 min. The fixed cells were permeabilized with cold methanol for 5 min, washed with PBS and incubated with PRDX3 (Abcam) and TOM20 (Santa Cruz) antibodies in 2% bovine serum albumin for 2 h at room temperature. The cells were again washed and incubated with fluorescent conjugated secondary antibodies, Alexa Fluor® 488 and Alexa Fluor® 555, for 1 h. The cells were washed and imaged by confocal microscopy (Zeiss LSM710).

Silencing RNA

Silencer® Select Validated silencing RNA (Ambion) targeting the human PRDX3 mRNA (antisense: AAUUCGUUAGCUUUGUCACta) and control silencing RNA were transfected into Daoy cells with Lipofectamine® RNAiMAX (Thermo Fisher Scientific) and incubated for different time periods (24–72 h).

Western blot

The cells were lysed with RIPA buffer (Thermo Fisher Scientific) containing proteasome inhibitors. The cells were then sonicated and centrifuged at 13 000*g* for 10 min at 4°C to remove cell debris. Proteins from the cell lysates were quantified using a BCA kit (Thermo Fisher Scientific). Forty micrograms of proteins were loaded into a 4–12% Bis-Tris acrylamide gel (Thermo Fisher Scientific) and transferred to a PVDF membrane. Membranes were probed with the following antibodies: PRDX3 (Thermo Fisher Scientific, PA3-752), PRDX5 (Invitrogen, MA5-29498), TOM20 (Santa Cruz), GAPDH (Santa Cruz) and TXN2 (Abcam).

H_2O_2 measurement

A total of 20 000 cells were cultured in a 96-well plate and incubated overnight. The medium was replaced the next day with 60 µl of fresh medium without FBS and incubated for 4 h. The H_2O_2 generated from the cells was measured using the Amplex® Red hydrogen peroxide assay kit (Thermo Fisher Scientific) following the manufacturer's protocol. Briefly, 50 µl of medium from the cell culture were plated into the wells of a black 96-well plate with 50 µl of the Amplex® Red assay kit reagents and incubated for 30 min at room temperature. Fluorescence was measured with a microplate reader (Biotek Synergy 2) using an excitation wavelength of 530 nm and fluorescence detection at 590 nm.

Cell viability assay

A total of 20 000 cells were plated into the wells of a white 96-well plate and incubated overnight. The cells were transfected with silencing RNA and incubated for 48 h. The cell viability was measured with the CellTiter-Glo® 2.0 kit (Promega). A 100 µl aliquot of CellTiter-Glo® 2.0 reagent was added to the cells and incubated for 10 min. The luminescence was measured with a microplate reader (Biotek Synergy 2).

Glutathione peroxidase activity

Glutathione peroxidase activity was measured from cell lysates using a calorimetric assay kit (Glutathione peroxidase activity assay kit, Abcam). The assay was performed according to the manufacturer's protocol. Briefly, 2 million cells were collected, lysed and centrifuged at 4°C to remove the cell debris. An assay mix containing NADPH, glutathione and glutathione reductase was prepared and incubated with 20 µg of cell lysates plated in triplicate in 96-well plates. Cumene hydroperoxide was added and the optical density (340 nm) was measured in kinetic mode for 15 min using a plate reader (Biotek Synergy 2).

Oxygen consumption rate

Oxygen consumption was measured at 37°C using a Seahorse XFp Extracellular Flux Analyser (Seahorse Bioscience). The cells were seeded at a density of 20 000 cells/100 μl/well into six different wells of an XFp cell culture plate (wells A and H contained media only). In addition, an XFp sensor cartridge for each cell plate was placed in an eight-well calibration plate containing 200 μl/well of sterile water and left to hydrate overnight at 37°C. On the following day, the water was replaced with pre-warmed XF Calibrant, at least 45–60 min prior to the assay. On the day of the assay, the cell culture medium from the cell plates was replaced with 175 μl/well of pre-warmed low-buffered Seahorse medium with no glucose followed by incubation at 37°C for at least 1 h to allow the temperature and pH of the medium to reach equilibrium before the first rate measurement. Measurements of endogenous respiration were followed by 1.25 μM of oligomycin, 2 μM of FCCP and 1 μM of rotenone plus antimycin A. All oxygen consumption rates and bioenergetic parameters were determined as indicated in the Excel report generated from Wave Software and were expressed as the percent of control cells. The results were normalized to micrograms of protein per well quantified after each Seahorse run, with the DC protein assay (Bio-Rad), according to the manufacturer's instructions.

Drosophila husbandry

Fly stocks were maintained at room temperature on a standard *Drosophila* diet (cornmeal, sugar and yeast). Crosses were maintained at 28°C and 60% humidity under a 12 h:12 h light-dark cycle. The inducible UAS-Prx3 RNAi strain VDRC27521 with RNAi construct 11779 (Prx3 RNAi) and the corresponding genetic control strain VDRC60000 (control) were obtained from the Vienna Drosophila Resource Centre (VDRC). VDRC27521 has an s19 value of 1.00, with zero predicted off-target effects. Ubiquitous Prx3 RNAi was induced by crossing the line (UAS-RNAi Prx3/CyO) to the ubiquitous Gal4 driver (UAS-Dicer-2; Actin-Gal4/CyO-GFP). An additional copy of UAS-Dicer-2, present in the driver line, enhanced the ubiquitous Prx3 RNAi efficiency. The original driver stock (BDSC25708) was obtained from the Bloomington Drosophila Stock Center (BDSC, Indiana University) and rebalanced with CyO-GFP. Pan-neuronal Prx3 RNAi was induced with the driver line w; UAS-Dicer-2; elav-Gal4, which was assembled in-house using w; UAS-Dicer-2 (VDRC60008) and w; elav-Gal4 stocks (kind gift from Pascal Heitzler). Muscle Prx3 RNAi was induced with w; Mef2-GAL4 (BDSC27390), and pan-glial Prx3 knockdown with w; repo-Gal4/TM6BHuTb (the original line, BDSC7415 was rebalanced with w; Sp/CyO-GFP; Dr/TM6bHuTb, a kind gift from Suzanne Eaton). For all experiments, Prx3 knockdown flies were compared to their appropriate genetic background control [the progeny of the promoter line crossed with the genetic background of the VDRC GD (VDRC60000) RNAi library]. A second available VDRC UAS-RNAi Prx3 line (VDRC105617) and its genetic control strain VDRC60100 were also recruited but did not result in reduced levels of *Prx3* mRNA when crossed to the ubiquitous Actin-Gal4 driver. Since this revealed the VDRC105617 RNAi line to be inefficient, we excluded it from the study and proceeded with the VDRC27521 RNAi strain that induced a robust, significant reduction in *Prx3* mRNA levels.

Verification of Prx3 knockdown efficiency by quantitative PCR

To evaluate the Prx3 knockdown efficiency, 4-day-old males of the appropriate genotypes were selected for RT-qPCR. Total RNA was purified from whole bodies using the PicoPure® RNA isolation kit (Thermo Fisher Scientific) according to manufacturer's protocol. Five animals were used per biological replicate. Quantitative PCR was performed as described[23] with the following adaptations. RNA was subjected to DNase treatment using the DNA-free kit (Ambion) before cDNA synthesis to avoid genomic contamination. Relative differences in Prx3 expression levels were calculated using the 2-ΔΔCt Livak method. To calculate ΔCt, the average Ct value for each sample was subtracted from the geometric mean Ct value of the reference genes RNA PolII and γTub23C. The primer sequences of RNA PolII were 5′- CGGCGATACTTCTCTCCAC-3′ and 5′-GACCAGCTAGGCGACATTC-3′, the primer sequences of γTub23C were 5′-TAATGGGCTCGGTCTACTCC-3′ and 3′-TGTCGAATACCTCT TCTTGCAG-5′ and the Prx3 primer sequences were 5′-GAAGACTA CAGGGGCAAGTACC-3′ and 5′-CGCTAAATGCAACAATTTCG-3′. For each genotype, six biological and two technical replicates were analysed.

Locomotion assay

To examine the walking behaviour of adult flies, aliquots of 15 male flies per genotype were collected at the day of eclosion and transferred to a new vial containing standard food. Tracking was carried out 3 days after collection during Zeitgeber Time 3–8 at room temperature as described previously.[24,25] The Ctrax output files were analysed in MATLAB to calculate the total distance and speed while moving parameters. All parameters were normalized against the average value of the corresponding genetic control strain that were run in parallel in the experiments. Distances were calibrated based on the arena diameter. For each genotype, a minimum of three biological replicates were analysed.

Eclosion

To induce Prx3 knockdown, *Prx3 RNAi/CyO*, males were mated to *UAS-dicer2; Actin-Gal4/CyO-GFP;* virgins, yielding progenies of three genotypes. Their expected ratios (33% Prx3 knockdown animals versus 66% CyO siblings or 50% control animals versus 50% CyO siblings) provided the basis for the evaluation of the eclosion rate. For this, the number of non-CyO Prx3 knockdown males and CyO siblings from five independent crosses was counted for five consecutive days.

Survival: *Drosophila*

For survival, at least 60 male flies were collected at the day of eclosion for each genotype and subsequently aged on standard fly food. Every 2–3 days adults were transferred to vials with fresh food and dead flies were counted until all had died.

Cell death immunofluorescence and microscopy

To detect cell death, brains of aged (20-day-old) male flies were dissected and fixed for 30 min in 3.7% PFA, rinsed twice in PBS and blocked for 2 h in PBS-Triton™ X-100 (0.6%, PBS-T) containing 10% NGS at room temperature. The brains were incubated with the primary antibody anti-Asp175 (Cell Signaling, 1:200) for 2 days at 4°C, labelling cleaved Caspase-3. The brains were washed five times for 10 min in PBS-T and incubated for 2 h with secondary antibodies (Alexa-568 red mouse, Life Technologies, 1:500) at room temperature. The brains were mounted in ProLong™ Gold Antifade reagent (Thermo Fisher Scientific). At least 10 images of the central brain were taken per genotype using a Zeiss Axio Imager fluorescence microscope (×40 magnification) with an apotome at a distance of 1 μm between the imaged focal planes. Asp175-positive cells in the central brain and central brain perimeter and area were quantified in Fiji.

Stress induction

Individual, 4-day-old male flies were placed in 65 mm × 5 mm glass tubes (Trikinetics) containing either standard food or standard food with 25 mM Paraquat to induce oxidative stress. Survival data were recorded with the Drosophila Activity Monitor (DAM) system (Trikinetics) and binned in 30-min intervals with DAMFileScan software (Trikinetics). Flies were considered dead when no more activity events were recorded. For each genotype, three biological replicates and a minimum of 10 technical replicates were analysed.

Statistical analysis

GraphPad Prism 5.0 software and the non-parametric *t*-test were used to calculate differences between genotypes. Survival curves were analysed with the Log-rank test (Mantel-Cox). *P*-values < 0.05 were considered to be significant. Annualized disease progression was estimated by the slope of a linear regression through all available SARA scores across individuals.

Data availability

Data supporting our results are available upon request.

Results

Deep phenotyping of PRDX3 disease including first longitudinal progression data

The PRDX3 patients described presented with early onset (median 21 years, range 13–22 years) cerebellar ataxia. This was frequently complicated by hyperkinetic movement disorders (3/5 patients) such as myoclonus, dystonia and/or tremor, and partly also mild hypokinetic movement features (2/5 patients) such as bradykinesia or hypomimia, which suggested damage of the basal ganglia system (for details on all phenotypic features, see Table 1). In contrast to many other autosomal-recessive ataxias,[26] there was no clinical or electrophysiological evidence of damage to the pyramidal tract or peripheral neurons in any of the five index subjects. Mild classical mitochondrial features were seen in only 1/5 patients, namely ptosis and COX-negative fibres (Patient 5), and none of the patients showed other classical features of mitochondrial diseases such as ophthalmoparesis, sensory neuropathy, epilepsy, hypoacusis, optic atrophy, diabetes or cardiomyopathy. Cognitive deficits were seen only in one patient (Patient 5: learning disabilities). Cerebellar atrophy on routine MRI was a ubiquitous feature present in all PRDX3 patients (5/5) across the different ages and ranges of disease duration (Fig. 1B–D), without clear-cut progression on visual inspection in those subjects where longitudinal routine MRI was available (e.g. 7-year follow-up MRIs of Patient 1; Fig. 1B and C). Brain atrophy extended beyond the cerebellum in 2/5 patients, here including the brainstem (1/5 patients, Patient 2) and the cortex (1/5 patients, Patient 3; parietal atrophy). This finding of recurrent extra-cerebellar damage in PRDX3 disease is further supported by the MRI findings of the two patients (Patients 2 and 3) showing bilateral symmetric T_2-hyperintense linear signals at the level of the medullary olives (Fig. 1E and F), compatible with (apparently non-hypertrophic) olivary degeneration, as often seen in early-onset mitochondrial diseases, in particular Leigh and Leigh-like syndromes.[27]

Disease evolution in PRDX3 spreads from gait ataxia (median onset 21 years) to upper limb ataxia (median onset 23 years) to dysarthria (median onset 25 years) and then dysphagia (median onset 30 years), all within a decade, suggesting a caudal-to-rostral spatial spread of disease. First preliminary prospective disease progression data [cross-sectional SARA data available for all (5/5) patients, longitudinal data available for 3/5 patients, with follow-up visits up to 6 years (median 5 years)] indicate a mean annualized increase of 0.44 SARA points per year (95% CI: 28–0.60)

Thus, while the spatial spread across effector levels towards speech and swallowing functioning was fairly quick, the severity of overall disease progression was relatively mild. Correspondingly, functional impairment remained mild to moderate before the age of 40 years (SDFS 2–3), while dependence on walking aids only occurred in Patient 3 after age 44 years

Identification of biallelic *PRDX3* variants in patients with cerebellar ataxia

Whole-exome sequencing was performed in five unrelated index individuals diagnosed with 'sporadic' (i.e. simplex) cerebellar ataxia (Table 1) and analysed by bioinformatics tools provided via the GENESIS platform.[22] This platform currently contains 10 477 whole exomes/genomes from individuals with different phenotypes, including 1750 individuals with cerebellar ataxia from the PREPARE consortium. We identified five unrelated affected individuals with cerebellar ataxia with recessive variants in *PRDX3* (GenBank: NM_006793.5) (Fig. 1A). The families originated from Germany, France, India and eastern Turkey, with a negative family history in all five patients but consanguineous background in two of five families. Mutations in other known ataxia genes were absent in all families. Two seemingly unrelated families originating from Kurdish Turkey (Families 1 and 2) showed the same homozygous missense variant c.604G>A (p.Asp202Asn). Two families showed loss-of-function variants: Family 3 carried a homozygous frameshift, c.240dupG (Ala114GlyfsTer3) and Family 4 had a homozygous stop-gain mutation, c.508C>T (p.Arg170Ter). Compound heterozygosity was identified in Family 5: a missense c.425C>G (Ala142Gly) and a splice-acceptor change, c.37-2A>G, which was predicted to abolish the intron 1 acceptor site leading to exon 2 skipping. All variants were located in the conserved PRX_Tyrp2cys domain of the protein (Fig. 2A and B). The missense mutations, Asp202Asn and Ala142Gly, were located at regions of high conservation across different species (Fig. 2C) with GERP scores equivalent to 5.19 and 4.9, respectively. Both missense mutations were predicted to be pathogenic according to most computation predictor tools including MutationTaster, MutationAssessor, SIFT and others. Further, applying the same filters in the GENESIS database (minor allele frequency gnomAD < 0.001), biallelic *PRDX3* variants were absent from our internal controls (8758 non-ataxia from whole exome/whole genome sequencing). A Fisher's exact test supported a significant enrichment of *PRDX3* biallelic variants in ataxia phenotypes compared to this control cohort of non-ataxia individuals in GENESIS, using the same filtering approach ($P = 0.0002$)

PRDX3 forms a dodecamer ring complex containing 12 identical PRDX3 subunits, as depicted by the 3D structure protein model built using Yasara (Fig. 2D). Interestingly, the Asp202Asn mutation was located at the dimer interface located between two PRDX3 subunits (Fig. 2E). The peroxiredoxin dimer interface was composed of conserved residues arranged in antiparallel beta-sheets, providing stability to the intermolecular redox-active disulphide bond region.[16,28] This suggested a possible dimerization interference and consequently protein complex assembly defect caused by the mutation. On the opposite side of the molecule, the mutated Ala142Gly was also located at the interface of adjacent subunits (Fig. 2F). Thus, based on this structural modelling data, both missense mutations were predicted to affect complex assembly.

Effects of PRDX3 mutations in patient fibroblasts

Skin fibroblasts were isolated from patients in order to investigate the effect of different *PRDX3* mutations in cells. The levels of PRDX3 expressed in fibroblast from five index patients were evaluated by western blot. The results revealed that PRDX3 was completely absent in four patients' fibroblasts, including Patients 1 and 2 with the missense mutation Asp202Asn, which was located at the protein dimer interface (Fig. 3A). This suggested that the missense mutation led to protein instability, probably due to interference in the dimer formation resulting in complete protein loss-of-function, as predicted by our structural modelling data. We observed that the healthy sister who was heterozygous for the Asp202Asn variant expressed about half the amount of PRDX3 protein, which suggested that one copy of the wild-type allele is sufficient to achieve a normal level of function. As expected, the loss-of-function mutations Ala114GlyfsTer3 and Arg170Ter, present in Patients 3 and 4, respectively, also led to PRDX3 depletion (Fig. 3A). The presence of a possible truncated protein was not detected, suggesting that the loss-of-function mutation led to nonsense-mediated mRNA decay. A faint band was detected in Patient 5, who carried a splice variant, c.37-2A>G, in *trans* with a missense variant, Ala142Gly. RT-PCR confirmed that splicing was affected Therefore, the band was likely to be a product of the missense variant, although we could not rule out the possibility of a leaky or incomplete splicing effect. To test whether the mutant protein (Asp202Asn) was being targeted for degradation by the proteasome system, fibroblasts were treated with a proteasome inhibitor. Western blots showed detectable levels of PRDX3 after proteasome inhibitor treatment, indicating that PRDX3 clearance was due in part to rapid degradation by the proteasome system (Fig. 3B). In contrast, the proteasome inhibitor did not recover any levels of PRDX3 in the patient with the frameshift mutation (Patient 3), confirming nonsense-mediated mRNA decay. We also analysed the levels of PRDX5, a paralogue of PRDX3 that is expressed partially in the mitochondria, peroxisomes and nucleus. Surprisingly, PRDX5 was reduced in four of five patients (Fig. 3A). This result indicated a coregulatory connection between PRDX3 and PRDX5. This finding opens the avenue for further investigations unravelling the link between PRDX3 and PRDX5 protein levels, indicating that both PRDX proteins might be co-regulated rather than compensate for each other.

Because H_2O_2 can also be reduced by another major oxidative stress defence mechanism, glutathione peroxidase, we decided to measure glutathione peroxidase activity in the patients' fibroblasts. Surprisingly, this was significantly reduced in all patients with PRDX3 mutations compared to the control fibroblasts (Fig. 3C

Table 1 Phenotypic features of the PRDX3 patients

Family	1	2	3	4	5
Demographics					
Current Age	36	36	55	32	40
Sex	Male	Male	Female	Male	Male
Ethnicity	Kurdish	Kurdish	German	Indian	French
Consanguinity	Unknown	Yes	Unknown	Yes	No
Genetics					
Mode of inheritance	Simplex	Simplex	Simplex	Simplex	Simplex
Allele 1	c.604G>A; p.Asp202Asn	c.604G>A; p.Asp202Asn	c.340dupG; p.Ala114GlyfsTer3	c.508C>T; p.Arg170Ter	c.425C>G; p.Ala142Gly
Allele 2	c.604G>A; p.Asp202Asn	c.604G>A; p.Asp202Asn	c.340dupG; p.Ala114GlyfsTer3	c.508C>T; p.Arg170Ter	c.37-2AA>G, p.Ser12fs
Disease onset and progression					
Gait ataxia, years	22	13	23	21	15
Upper limb ataxia, years	24	20	23	21	30
Dysarthria, years	25	20	31	21	30
Dysphagia, years	25	–	31	30	38
SARA score (age)	13 (30), 14 (35)	11 (30), 13.5 (36)	21.5 (54)	8.5 (31)	14 (36), 14 (37), 15 (39)
Phenotypic features					
Age at last exam, years	35	36	54	31	39
Oculomotor signs	Saccadic pursuit, hypermetric saccades	Hypermetric saccades, gaze-evoked nystagmus	Saccadic pursuit, hypermetric saccades	Saccadic pursuit, hypermetric saccades	Saccadic pursuit
Cerebellar dysarthria	Yes	Yes	Yes	Yes	Yes
Hypokinetic features	No	No	Hypomimia	No	Bradykinesia
Hyperkinetic features	Myoclonus of trunk, arms and legs	No	Postural tremor, cervical dystonia	No	Postural tremor, cervical myoclonus dystonia
Pyramidal signs	No	No	No	No	Patellar reflex ↑
Muscle weakness	No	No	No	No	Ptosis
Sensory impairment	No	No	No	No	No
Cognitive impairment	No	No	No	No	Learning disabililty in childhood
MRI	Cerebellar atrophy	Cerebellar and brainstem atrophy	Cerebellar atrophy, mild parietal atrophy	Cerebellar atrophy	Cerebellar atrophy
Diagnostic features	NCS and MEP normal	NCS normal	NCS, MEP and SEP normal	NCS normal	NCS normal; muscle biopsy: some COX-negative fibres

MEP = motor evoked potential; NCS = nerve conduction study; SEP = sensory evoked potential.

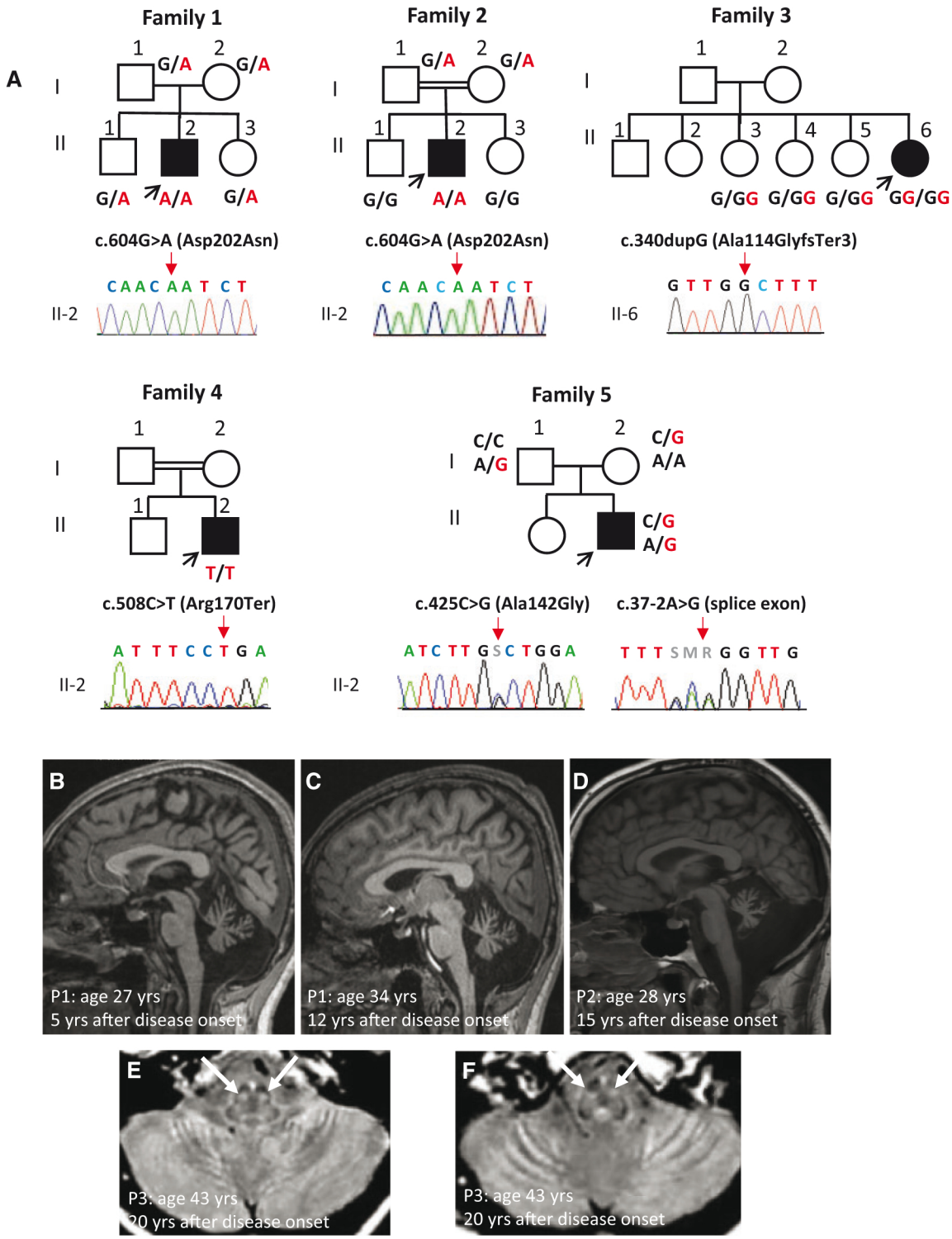

Figure 1 Cerebellar ataxia families with recessive mutations in *PRDX3*. (**A**) Pedigrees of cerebellar ataxia families showing segregation of recessive *PRDX3* variants: Families 1 and 2, Asp202Asn; Family 3, Ala114GlyfsTer3; Family 4, Arg170Ter and Family 5, c.37-2A>G and Ala142Gly. (**B–F**) Brain MRI shows marked cerebellar atrophy [**B**, Patient 1 (P1 = index patient of Family 1); **D**, Patient 2 (P2 = index patient of Family 2); both sagittal T_1 MRI], without clear-cut progression on 7 years follow-up (**B** versus **C**, both Patient 1, sagittal T_1 MRI), and bilateral symmetric T_2 hyperintensity at the level of the medullary olive, present across different slices [**E** and **F**, both Patient 3 (P3 = index patient of Family 3) axial T_2 MRI].

and D). This result indicated that both pathways were cross-linked and might act in concert in the process of H_2O_2 detoxification.

To explore the effect of the recurrent, functionally interesting p.Asp202Asn variant, we evaluated the effect of this particular *PRDX3* mutation on mitochondrial function by determining the oxygen consumption rate using the Seahorse XFp. Maximal respiratory capacity was achieved by treatment with the mitochondrial oxidative phosphorylation uncoupler FCCP to reach the maximal oxygen consumption rate. Although we did not detect a significant difference in the basal respiration levels between the controls and patient (Family 1), the maximal respiration and spare respiratory capacity were significantly reduced (Fig. 3F–H). The

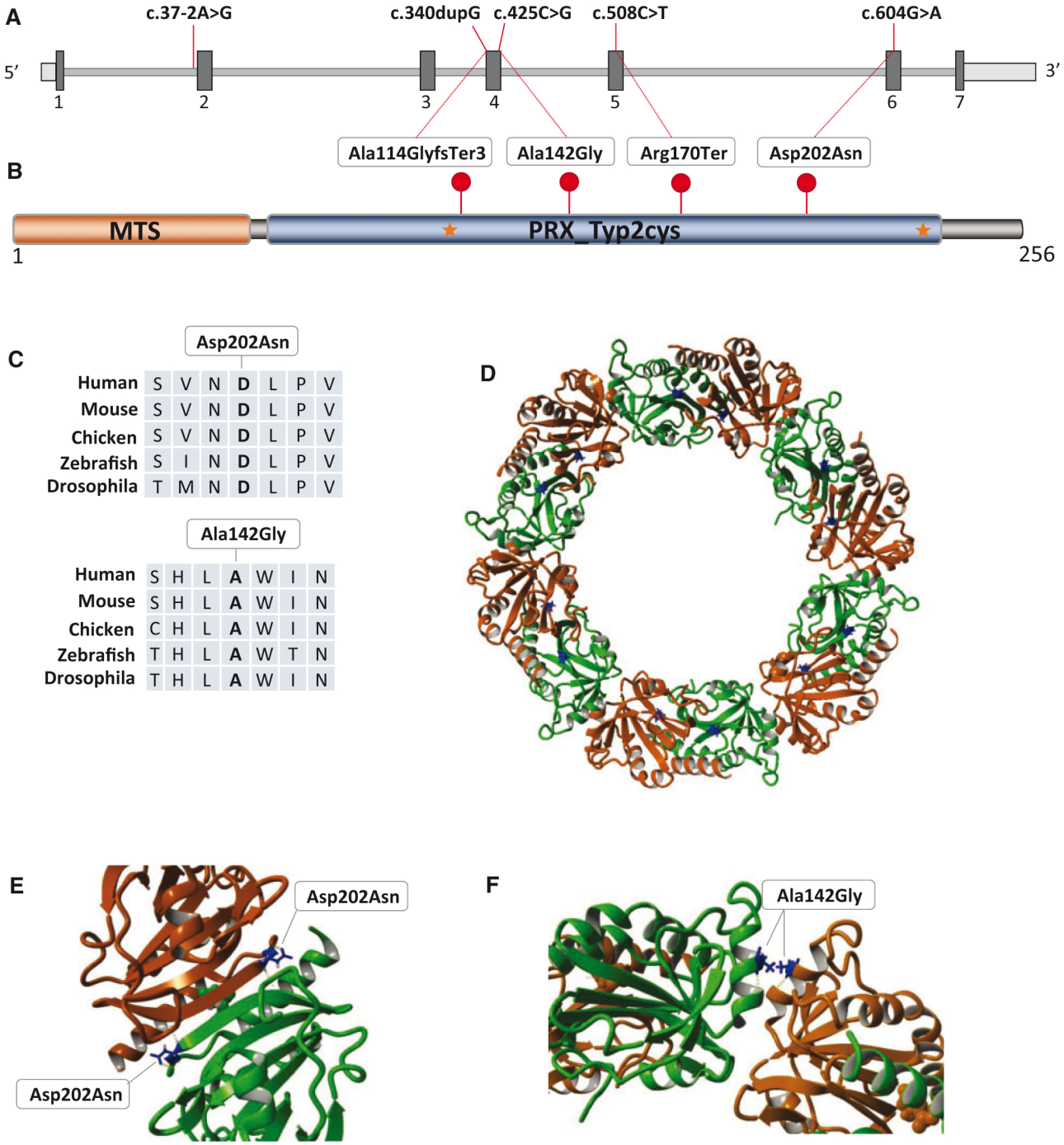

Figure 2 Positional *in silico* analysis of *PRDX3* mutations. (**A**) Diagram showing *PRDX3* mRNA and cDNA mutations mapped to their corresponding locations. Dark rectangles represent exons 1–7. (**B**) Diagram showing PRDX3 protein domains, including the mitochondrial targeting sequence (MTS) and the PRX_Typ2cys domain. Amino acid changes are displayed inside boxes and their corresponding protein locations are represented by red lollipops. Stars represent active site resolving cysteines. (**C**) Missense *PRDX3* mutations, Asp202Asn and Ala142Gly are located in a conserved region across different species. (**D**) A 3D model of human ring-like PRDX3 oligomer (dodecamer) composed and depicted with Yasara. Each PRDX3 subunit is shown in alternating colours (green and brown). (**E** and **F**) The protein dimer interface between two PRDX3 subunits showing the identified missense mutations, Asp202Asn and Ala142Gly.

decreased levels of those parameters indicated that the ATP-generating capacity could be compromised, which might become limiting, specifically under stress conditions where there is high ATP demand.

Effects of PRDX3 knockdown in human cerebellar medulloblastoma

Human cerebellar medulloblastoma cells, Daoy (ATCC), were used to assess the functional consequences of *PRDX3* downregulation.

To demonstrate that *PRDX3* is endogenously localized in mitochondria, we performed an immunofluorescence analysis. Daoy cells were co-labelled for PRDX3 and the mitochondrial marker TOM20, confirming the localization of PRDX3 in the mitochondria (Fig. 4A). To determine the effects of PRDX3 downregulation, cells were transfected with silencing RNA against PRDX3, while a scrambled silencing RNA was used as a negative control. Western blots confirmed the efficient knockdown of PRDX3 after 24–72 h of transfection (Fig. 4B). We observed that PRDX3 knockdown

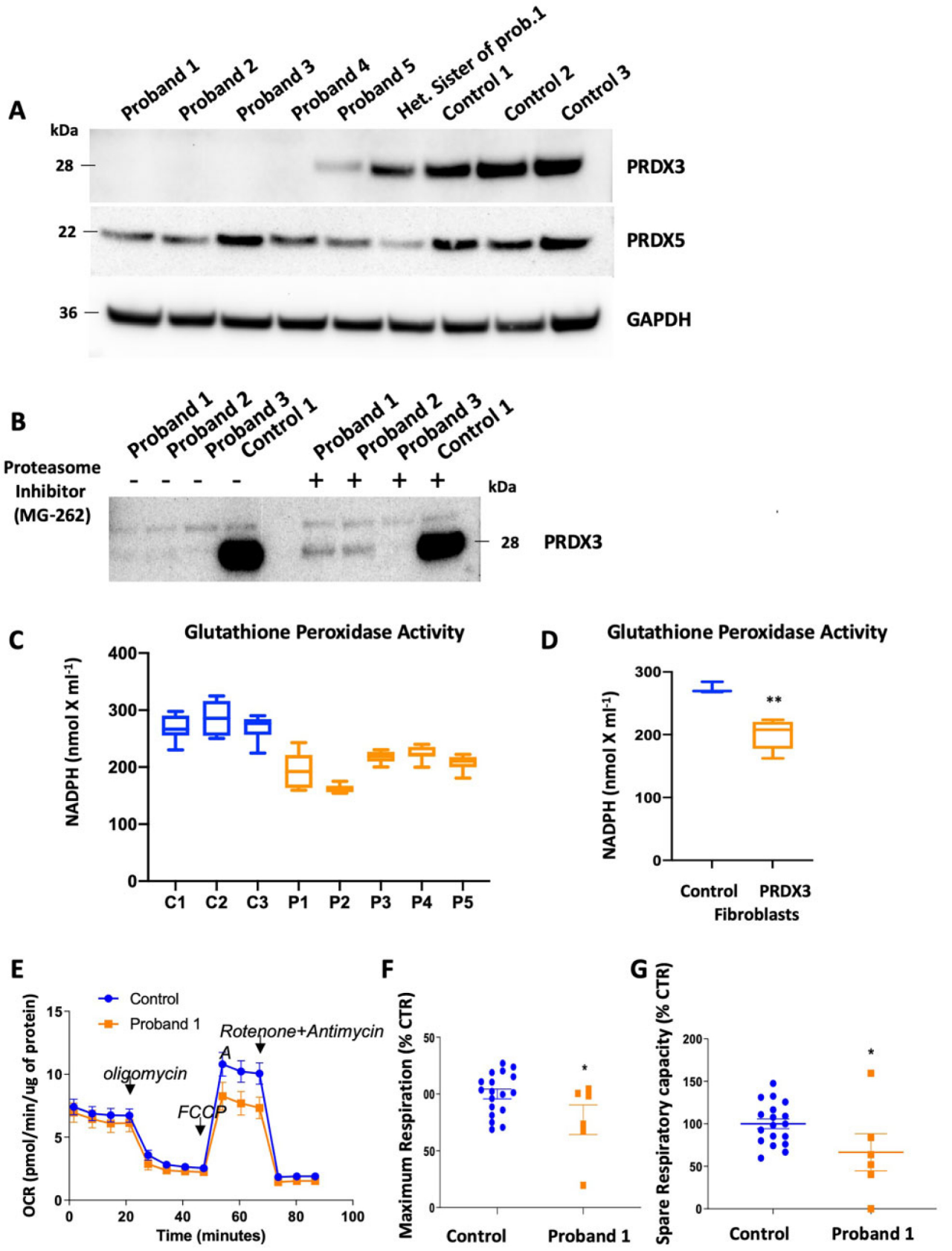

Figure 3 Studies on the fibroblasts of PRDX3 patients. (**A**) Western blot of fibroblasts from five patients with *PRDX3* mutations probed with PRDX3, PRDX5 and GAPDH antibodies. PRDX3 was absent from Probands 1–4. A faint band was detected in Proband 5, which carried a compound heterozygous splice-variant and missense variant. (**B**) Western blot from fibroblasts treated with the proteasome inhibitor MG262. In the presence of MG262, the PRDX3 band was detected in both Proband 1 and Proband 2 with the missense variant (Arg202Asn) but not in Proband 3 with a loss-of-function variant (Ala114GlyfsTer3). (**C**) Glutathione peroxidase activity was measured kinetically by the rate of depletion of NADPH in a calorimetric assay.

(continued)

resulted in significantly decreased cell viability, which was measured by ATP luminescence. Cell viability was reduced by 11.4% ($P < 0.0001$) compared to the control (Fig. 4C). This result confirmed previously reported data showing decreased cell viability as a result of PRDX3 knockdown.[29] PRDX3 knockdown also resulted in significantly increased levels (1.8-fold) of H_2O_2 in the cell media, measured with the Amplex® Red fluorescent probe (Fig. 4D), indicating the important role of PRDX3 as a cellular antioxidant. To assess the ability of PRDX3 knockdown cells to deal with oxidative stress, cells were treated with concentrations ranging from 200 μM to 600 μM of H_2O_2. We observed that the cells treated with PRDX3 silencing RNA were significantly more prone to cell death triggered by H_2O_2 compared to cells treated with control silencing RNA (Fig. 4E), suggesting that the PRDX3-deficient cells are more susceptible to oxidative stress.

Drosophila models of PRDX3 deficiency

To gain independent support for the implication of PRDX3 in autosomal-recessive ataxia pathology, we used the fruit fly *Drosophila melanogaster*, a well-established model organism to study degenerative movement disorders including cerebellar ataxia.[30,31] *Drosophila* contains a poorly characterized one-to-one orthologue of PRDX3, Prx3. *Drosophila* Prx3 shares 58% of overall sequence identity at amino acid level with human PRDX3, with particular high conservation of the PRDX3 active site residues (in the catalytic triad and the peroxidatic and resolving cysteines) and the amino acids that make up the PRDX3-PRDX3 dimerization interface.[32] *Drosophila* Prx3 is broadly and highly expressed throughout development.[33,34] Prx3 expression levels peak during early larval and late pupa stages.[33,34]

In the absence of *Prx3* mutants, we modelled the loss of human PRDX3 expression by inducing ubiquitous Prx3 knockdown in *Drosophila* using the UAS-Gal4 system, the ubiquitous promotor line Actin-Gal4 driver, and an UAS-RNAi line (VDRC27521) targeting the C-terminal part of *Prx3* mRNA. Relative *Prx3* mRNA expression levels in Prx3 knockdown animals were reduced to 46% ($P = 0.002$), compared to their genetic background controls (Fig. 5A).

Knockdown of Prx3 in *Drosophila* affects lifespan, confers susceptibility to oxidative stress and induces brain degeneration

Induction of ubiquitous Prx3 knockdown by crossing driver (UAS-Dicer-2; Actin-Gal4/CyO-GFP) and inducible Prx3 RNAi lines (UAS-Prx3 RNAi/CyO) resulted in the expected ratio of progenies and was thus fully viable to adulthood (Fig. 5B). Male adults were carefully monitored for defects in lifespan. Ubiquitous Prx3 knockdown induced a mild, although significant ($P = 0.006$), reduction in lifespan (Fig. 5C). As can be expected from loss of peroxiredoxin function,[35,36] the survival of Prx3 knockdown models was reduced ($P = 0.0004$) upon exposure to oxidative stress, as induced by feeding with Paraquat (Fig. 5D).

To evaluate whether the loss of Prx3 led to increased cell death in the brain, we performed immunolabelling on brains ubiquitous knockdown animals from 20 days of age using an antibody against cleaved Caspase-3 at Asp175, an early marker of apoptosis. Knockdown of Prx3 led to a significant increase ($P < 0.05$) of activated Caspase-3-positive cells in the central brain, suggesting that loss of Prx3 induced degeneration (Fig. 5E and F). Despite the increase in apoptotic cells in Prx3 knockdown brains of ubiquitous knockdown animals from 20 days of age, we did not detect a decrease in central brain area or perimeter (Fig. 5G and H).

Knockdown of *Drosophila* Prx3 affects coordinated motor behaviour

To evaluate the consequences of loss of Prx3 function to coordinated locomotor behaviour, we traced the locomotor paths of ubiquitous Prx3 RNAi fly models and controls over time in an open-field arena (Fig. 6A–C). Ubiquitous Prx3 knockdown resulted in a significantly shorter distance covered in a given time interval (15% reduction, $P < 0.01$) compared to the controls (Fig. 6B). In addition, during periods of motion, ubiquitous Prx3 RNAi animals showed reduced velocity (16% reduction, $P < 0.001$) compared to the control animals (Fig. 6C). Thus, loss of Prx3 in *Drosophila* affected motor function.

Since locomotor function depends on communication between several different cellular substrates, we made use of the flexibility of the Gal4-UAS system to explore whether Prx3 function in neurons, glia or muscles underlies the motor phenotypes of the ubiquitous Prx3 RNAi model. Prx3 knockdown in neurons and glia, but not in muscles, significantly affected motor behaviour in the open-field arena (Fig. 6D–E), indicating selective susceptibility of CNS constituents for Prx3 deficiency and associated reduced antioxidant capacity. Upon pan-neuronal Prx3 RNAi, distance covered over time was reduced by 14% ($P < 0.01$) with velocity during periods of moving being reduced by 13% compared to genetic control animals ($P < 0.001$, Fig. 6D and E). Pan-glial Prx3 RNAi significantly reduced the distance covered by 7% ($P < 0.01$) and velocity during periods of moving by 8% ($P < 0.001$, Fig. 6D and E). Together, these results illustrated that Prx3 function in the CNS is essential to normal motor function.

Discussion

Many neurological diseases, including ataxias, are associated with reactive oxygen species-induced neurological deterioration, which indicates that CNS is particularly vulnerable to oxidative stress.[5] Reactive oxygen species are important signalling molecules; however, they cause cell damage when their concentrations are not tightly controlled and exceed the cellular antioxidant capacity. Here we demonstrate that mutated *PRDX3*, a peroxiredoxin that plays a major role in H_2O_2 detoxification, is associated with human disease, presenting a new cerebellar ataxia gene. The associated disease is characterized by an early onset, mild-to-moderate (0.44 SARA/points per year) progressive ataxia with variable additional hyper- and hypokinetic movement disorders and involvement of the brainstem, medullary olive and parietal cortex. Yet classical clinical signs of a mitochondrial disease are rare (as is often the case in nuclear-encoded mitochondrial diseases).

Figure 3 Continued
The fibroblasts from all of the PRDX3 patients showed decreased levels of glutathione peroxidase activity compared with the control fibroblasts. (**D**) Combined glutathione peroxidase activity comparing the averages of all probands (Probands 1–5) and all control fibroblasts (controls 1–3). *T*-test, $P < 0.01$. (**E** and **F**) The oxygen consumption rate measured by Seahorse in the presence of FCCP to achieve maximum respiration. Proband 1 (homozygous Arg202Asn PRDX3 variant) showed decreased maximum respiration relative to the control. (**G**) Spare respiratory capacity, defined as the difference between maximal respiration and basal respiration, was decreased in Proband 1 compared to the control. Statistical analysis was performed using the *t*-test, $P < 0.05$, $n = 6$ (triplicates of each condition were run on each plate).

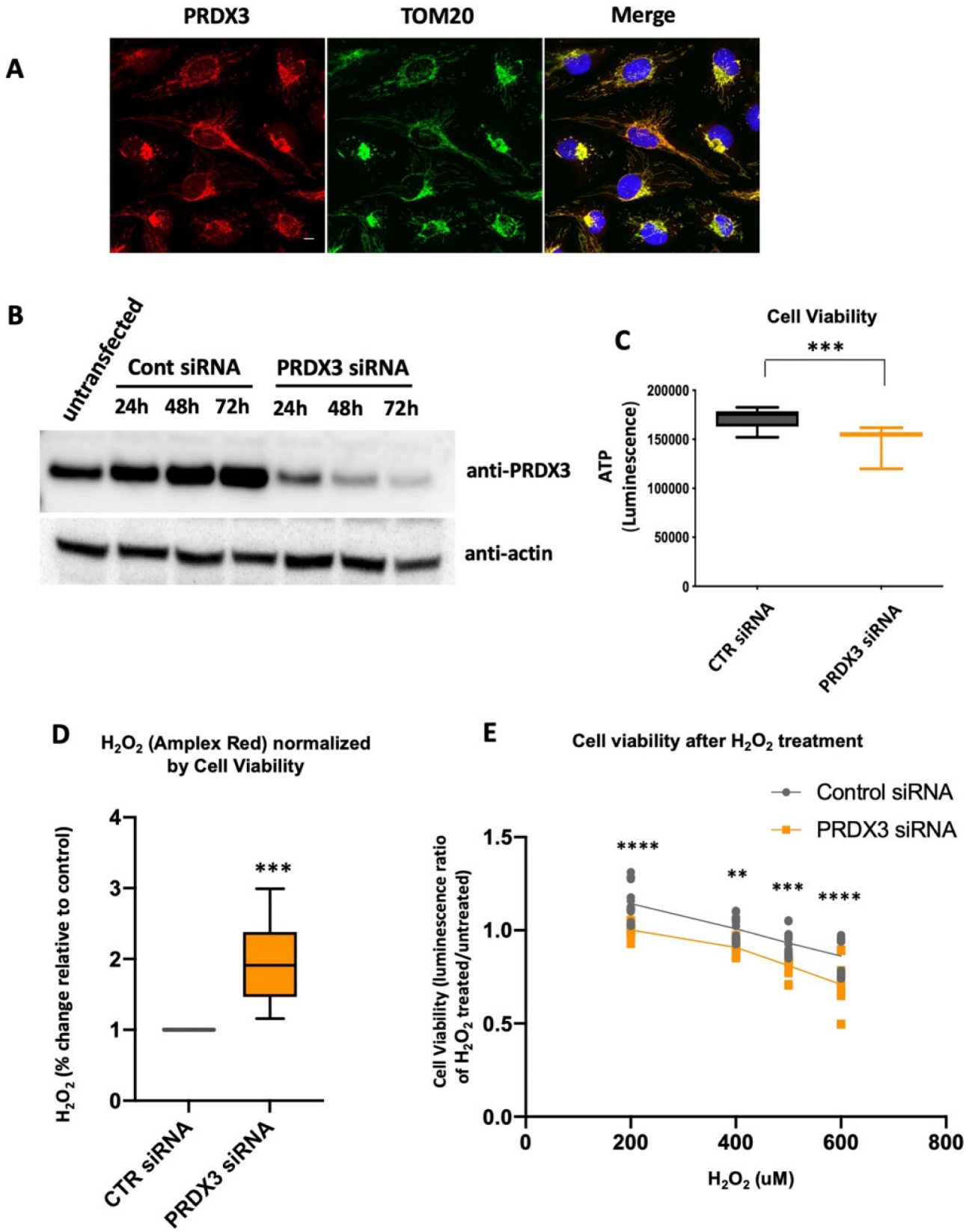

Figure 4 Studies with PRDX3 knockdown in cerebellar medulloblastoma (Daoy). (**A**) Immunofluorescence confocal microscopy showed PRDX3 (red) co-localization (yellow) with the mitochondrial marker Tom20 (green) by confocal microscopy in cerebellar medulloblastoma. (**B**) Western blot of cells treated with control and PRDX3 silencing RNAs at different time points. PRDX3 was efficiently knocked down after 24 h of treatment. (**C**) Cell viability measured by ATP luminescence showed decreased cell viability (11%) in cells treated with PRDX3 silencing RNA, reflecting increased cell death ($n = 24$, paired t-test, $P < 0.0001$). (**D**) Levels of H_2O_2 measured by Amplex red showed a significant increase of H_2O_2 in cells treated with *PRDX3* targeted silencing RNA ($n = 8$, t-test, $P < 0.001$). (**E**) Cell viability measured in cells treated with different concentrations of H_2O_2 (in μM) showed decreased cell viability in PRDX3 knockdown cells ($n = 16$ for each group). Statistical analysis was performed by two-way ANOVA with Sidak's multiple comparisons test (**$P = 0.0029$, ***$P = 0.0002$, ****$P < 0.0001$).

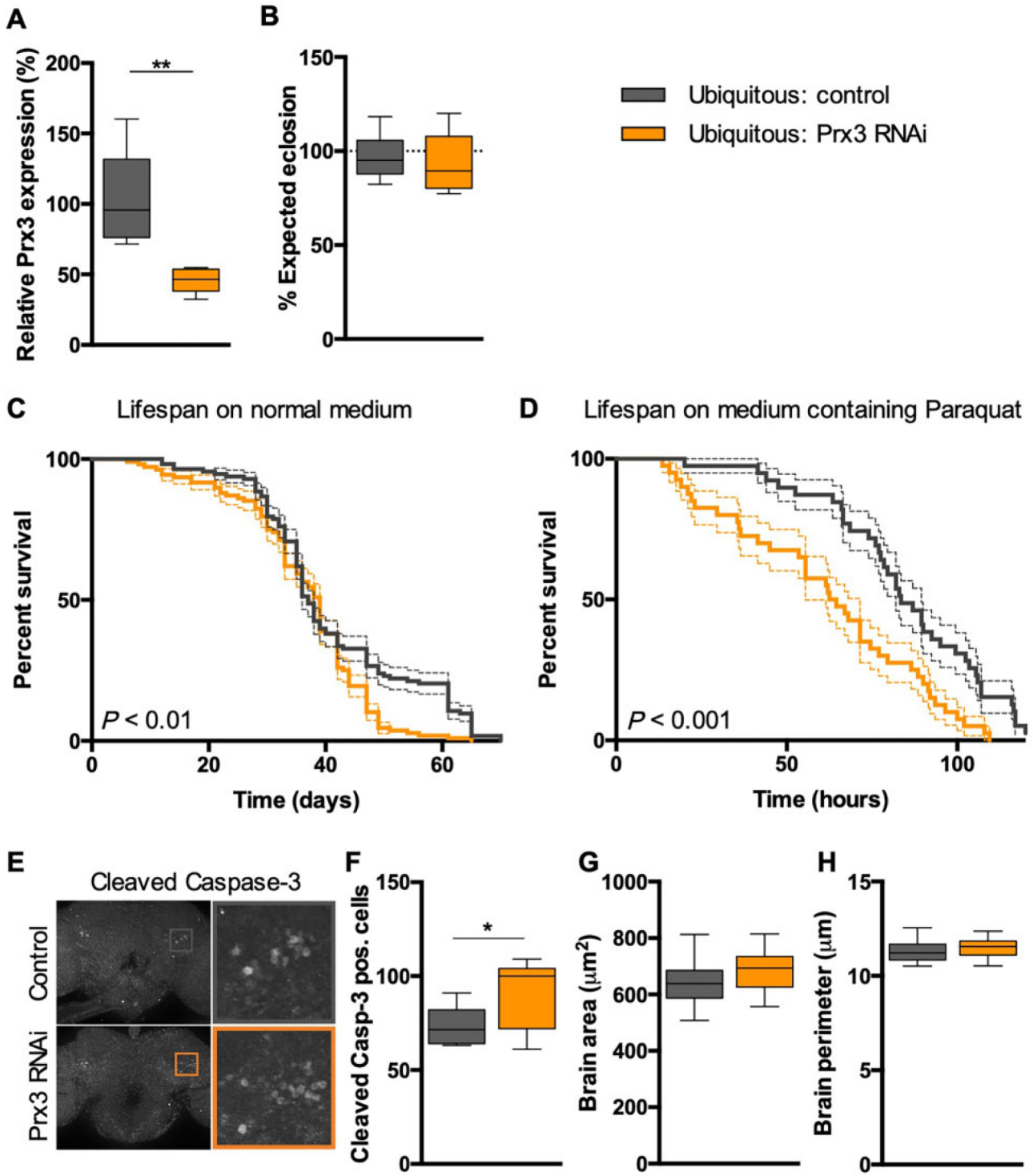

Figure 5 Modelling loss of Prx3 function in *Drosophila* decreases lifespan. (**A**) Relative Prx3 expression in male control (dark grey, genotype: UAS-Dicer-2/Y; Actin-Gal4/+) and Prx3 ubiquitous RNAi (orange, genotype: UAS-Dicer-2/Y; Actin-Gal4/Prx3 RNAi;) flies determined by quantitative PCR. Min-to-max box plots represent average of six independent biological replicates. (**B**) The expected eclosion rate of male flies (in %) from the control and Prx3 RNAi crosses. Min-to-max box plots represent average of five biological replicates. (**C**) Kaplan-Meier curve showing survival (in %) over days past eclosion of male control and Prx3 ubiquitous knockdown flies. Error bars indicate the standard error (SE). (**D**) Kaplan-Meier curve showing survival (in %) over time (in h) of male control and Prx3 RNAi flies upon paraquat exposure (drug that induces reactive oxygen species). Error bars represent the SE. (**E**) Immunolabelling of brains of control and ubiquitous Prx3 knockdown flies using an antibody against cleaved Caspase-3 at Asp175, an early marker of apoptosis. Knockdown of Prx3 showed an increased number of activated Caspase-3-positive cells in brain. Single optical sections are shown. (**F**) Min-to-max box plots displaying average number of cells in the central brain that were positive for the cleaved Caspase-3 Asp175 marker. (**G**) Area (μm^2) of the central brains of Prx3 RNAi and control flies. (**H**) The central brain perimeter in μm of Prx3 RNAi and control flies. (**H–I**). The brains measured were the same as those used for the quantification of cleaved Caspase-3 cells. $^{*}P < 0.05$, $^{**}P < 0.01$. $P < 0.001$ in **C** and **D**.

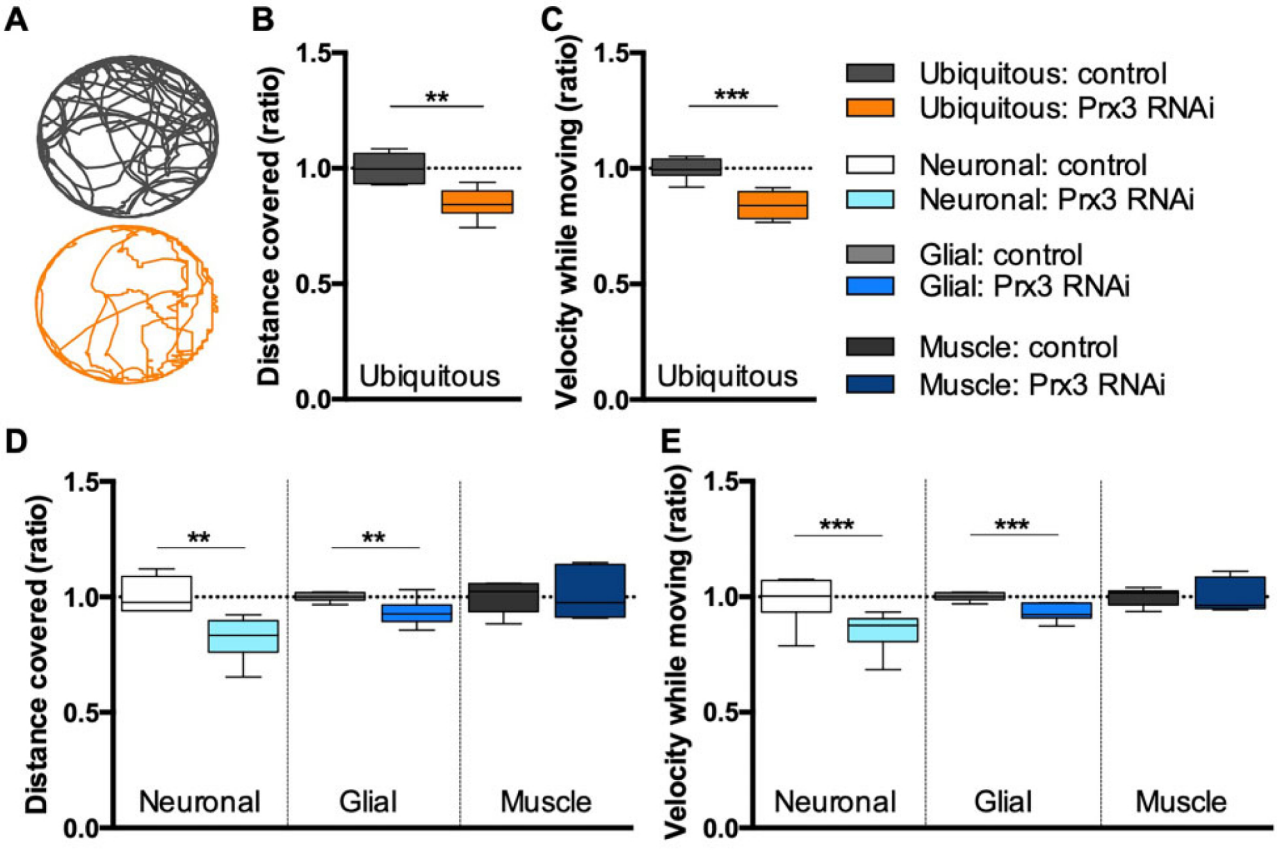

Figure 6 Modelling loss of Prx3 function in *Drosophila* affects motor behaviour. (**A**) Locomotion trajectories of representative control (dark grey) and ubiquitous Prx3 RNAi (orange) flies. (**B**) Min-to-max box plots displaying total distance covered by ubiquitous Prx3 RNAi and control flies during locomotion tracking. (**C**) Min-to-max box plots displaying the normalized speed while moving of ubiquitous Prx3 RNAi and control flies during locomotion tracking. (**D**) Min-to-max box plots displaying normalized total distance walked for pan-neuronal, pan-glial and muscular Prx3 RNAi and control flies. Genotypes: white = ; Dcr2/+; Elav-Gal4/+. Light blue = ; Dcr2/Prx3 RNAi; Elav-Gal4/+. Light grey = ; Repo-Gal4/+;. Blue = ; Repo-Gal4/Prx3 RNAi;. Black-grey = ; Mef2-Gal4/+;. Dark blue = ; Mef2-Gal4/Prx3 RNAi;. (**E**) Min-to-max box plots displaying normalized speed while moving during locomotion tracking of pan-neuronal, pan-glial and muscular Prx3 RNAi and control flies. (**B–E**) All conditions are normalized to the respective controls. The colour code is provided in **C** (*right*). $^{**}P < 0.01$, $^{***}P < 0.001$.

PRDX3 is localized in the mitochondria, which is the major source of free radicals generated by electron leakage from the respiratory chains during oxidative phosphorylation. Ablation of PRDX3 in mice has been shown to cause decreased physical strength, decreased mitochondrial copy number in the skeletal muscles and loss of hippocampus cells as a result of oxidative stress and mitochondrial impairment.[37] Although mice were not reported to develop ataxia, a more detailed evaluation of the cerebellum and olivary bodies should be reconsidered.

PRDX3 individuals carried recessive loss-of-function mutations resulting in depletion of PRDX3 protein, consequently rendering cells more susceptible to oxidative damage. Two probands from different families with the same ethnic background shared the same homozygous variant, Asp202Asn, which was positioned right at the protein dimer interface, created mainly by the formation of an antiparallel β-sheet. Residues positioned at the dimer interface are critical for stability of intermolecular redox-active disulphide bond formation,[16,28] because six PRDX3 dimers assemble to form a ring-like structure. Absence of PRDX3 protein in the patients' fibroblasts with the Asp201Asn mutation indicated protein instability probably due to disruption of the protein interface and oligomerization assembly.

In addition, our studies revealed decreased levels of maximal mitochondrial respiration and of 'spare respiratory capacity' in patient fibroblasts, indicating that mitochondria can be compromised under conditions (and in tissues) of high energy demand. The impaired mitochondrial metabolism in combination with accumulation of increased levels of H_2O_2 could be considered a possible pathological disease mechanism in our patients. This is supported by other studies that have reported induced oxidative stress and mitochondrial dysfunction upon *PRDX3* knockdown.[38] Our results also showed decreased glutathione peroxidase activity in all PRDX3 fibroblasts relative to control fibroblasts. This indicated that loss of PRDX3 interferes with the glutathione peroxidase pathway, probably due to crosstalk between electrons that flow between the two pathways.[18] Likewise, it has been reported that knockdown of PRDX6, another peroxiredoxin, also results in decreased glutathione peroxidase activity in lung cancer cells.[39] Glutathione is a major protective agent against peroxide oxidative damage that has also been proposed to be involved in the pathogenesis of some neurodegenerative diseases. Lower levels of glutathione have been reported in patient with amyotrophic lateral sclerosis, Parkinson's disease, Alzheimer's disease and other neurodegenerative diseases.[40–42] Moreover, we showed that PRDX3 downregulation in cerebellar medulloblastoma resulted in significantly decreased cell viability accompanied by increased accumulation of H_2O_2, supporting oxidative stress as the underlying pathological mechanism.

Our *in vivo* studies using *Drosophila* as a model also support the pathological effects due to *PRDX3* ablation. Knockdown of

Drosophila Prx3 resulted in decreased lifespan, increased susceptibility to oxidative stress and induced brain degeneration. Moreover, ubiquitous loss of Prx3 in *Drosophila* resulted in motor behaviour defects, characterized by aberrant locomotion trajectories which, as we demonstrate here, are due to increased neuronal and glial susceptibility to Prx3 deficiency. Our established *Drosophila* models and characterized phenotypes can be exploited for future preclinical treatment approaches.

PRDX3 is a thioredoxin-dependent peroxide reductase, and when oxidized, PRDX3 needs to be subsequently reduced by TXN2. Interestingly a null mutation in TXN2 has been shown recently to cause an early-onset neurodegenerative disorder with severe cerebellar atrophy and other additional clinical features in a single reported patient.[18] This TXN2-deficient patient had increased amounts of PRDX3 in its dimeric (oxidized) state. The authors also demonstrated that supplementation with antioxidants improved cell viability and mitigated clinical symptoms by reducing cellular levels of reactive oxygen species.[18] Further supporting and adding to these findings, our study now emphasizes a common cerebellar ataxia pathological mechanism associated with the mitochondrial antioxidant PRDX3-TXN2 pathway, suggesting the cerebellum to be particularly vulnerable to defects in this pathway. Antioxidant treatment should be further evaluated systematically in patients with *PRDX3* mutations.

Acknowledgements

We thank Mrs Selina Reich and Manuela Hauser (Tübingen, Germany) and the cell and DNA bank of the Hertie Institute for Clinical Brain Research (Tübingen, Germany) and of the ICM (Paris, France) for their technical support in genetic sequencing and fibroblast culturing.

Funding

This project was supported, in part, via the European Union's Horizon 2020 research and innovation program by the BMBF under the frame of the E-Rare-3 network PREPARE (01GM1607 to M.S., G.S, M.K., M.A., A.S., and as an associated partner S.Z.) and grant 779257 "Solve-RD" (to M.S. and G.S.) and the Association Connaitre les Syndromes Cérébelleux (to G.S.). We thank Mélanie Papin and Marie Coutelier for their help in genetic analysis. We also thank The Genesis Project foundation for access to the GENESIS platform for extensive data analyses. L.S., M.S., G.S. and A.D. are members of the European Reference Network for Rare Neurological Diseases, Project ID No 739510.

Competing interests

The authors report no competing interests.

References

1. Diener HC, Dichgans J. Pathophysiology of cerebellar ataxia. *Mov Disord*. 1992;7:95-109.
2. Synofzik M, Nemeth AH. Recessive ataxias. *Handb Clin Neurol*. 2018;155:73-89.
3. Synofzik M, Puccio H, Mochel F, Schols L. Autosomal recessive cerebellar ataxias: Paving the way toward targeted molecular therapies. *Neuron*. 2019;101:560-583.
4. Salman MS. Epidemiology of cerebellar diseases and therapeutic approaches. *Cerebellum*. 2018;17:4-11.
5. Eidhof I, van de Warrenburg BP, Schenck A. SnapShot: Biology of genetic ataxias. *Cell*. 2018;175:890-890.e1.
6. Schmucker S, Puccio H. Understanding the molecular mechanisms of Friedreich's ataxia to develop therapeutic approaches. *Hum Mol Genet*. 2010;19:R103-R110.
7. Seznec H, Simon D, Bouton C, et al. Friedreich ataxia: The oxidative stress paradox. *Hum Mol Genet*. 2005;14:463-474.
8. Lodi R, Hart PE, Rajagopalan B, et al. Antioxidant treatment improves in vivo cardiac and skeletal muscle bioenergetics in patients with Friedreich's ataxia. *Ann Neurol*. 2001;49:590-596.
9. Lax NZ, Hepplewhite PD, Reeve AK, et al. Cerebellar ataxia in patients with mitochondrial DNA disease: A molecular clinicopathological study. *J Neuropathol Exp Neurol*. 2012;71:148-161.
10. Schulte C, Synofzik M, Gasser T, Schols L. Ataxia with ophthalmoplegia or sensory neuropathy is frequently caused by POLG mutations. *Neurology*. 2009;73:898-900.
11. Synofzik M, Srulijes K, Godau J, Berg D, Schols L. Characterizing POLG ataxia: Clinics, electrophysiology and imaging. *Cerebellum*. 2012;11:1002-1011.
12. Bargiela D, Shanmugarajah P, Lo C, et al. Mitochondrial pathology in progressive cerebellar ataxia. *Cerebellum Ataxias*. 2015;2:16.
13. Stendel C, Neuhofer C, Floride E, et al.; ATP6 Study Group. Delineating MT-ATP6-associated disease: From isolated neuropathy to early onset neurodegeneration. *Neurol Genet*. 2020;6:e393.
14. Haugen AC, Di Prospero NA, Parker JS, et al. Altered gene expression and DNA damage in peripheral blood cells from Friedreich's ataxia patients: Cellular model of pathology. *PLoS Genet*. 2010;6:e1000812.
15. De Simoni S, Goemaere J, Knoops B. Silencing of peroxiredoxin 3 and peroxiredoxin 5 reveals the role of mitochondrial peroxiredoxins in the protection of human neuroblastoma SH-SY5Y cells toward MPP + . *Neurosci Lett*. 2008;433:219-224.
16. Yewdall NA, Venugopal H, Desfosses A, et al. Structures of human peroxiredoxin 3 suggest self-chaperoning assembly that maintains catalytic state. *Structure*. 2016;24:1120-1129.
17. Nonn L, Williams RR, Erickson RP, Powis G. The absence of mitochondrial thioredoxin 2 causes massive apoptosis, exencephaly, and early embryonic lethality in homozygous mice. *Mol Cell Biol*. 2003;23:916-922.
18. Holzerova E, Danhauser K, Haack TB, et al. Human thioredoxin 2 deficiency impairs mitochondrial redox homeostasis and causes early-onset neurodegeneration. *Brain*. 2016;139:346-354.
19. Wonsey DR, Zeller KI, Dang CV. The c-Myc target gene PRDX3 is required for mitochondrial homeostasis and neoplastic transformation. *Proc Natl Acad Sci U S A*. 2002;99:6649-6654.
20. Schmitz-Hubsch T, Du Montcel ST, Baliko L, et al. Scale for the assessment and rating of ataxia: Development of a new clinical scale. *Neurology*. 2006;66:1717-1720.
21. Traschutz A, Schirinzi T, Laugwitz L, et al. Clinico-genetic, imaging and molecular delineation of COQ8A-Ataxia: A multicenter study of 59 patients. *Ann Neurol*. 2020;88:251-263.
22. Gonzalez M, Falk MJ, Gai X, Postrel R, Schule R, Zuchner S. Innovative genomic collaboration using the GENESIS (GEM.app) platform. *Hum Mutat*. 2015;36:950-956.
23. Mukhopadhyay A, Kramer JM, Merkx G, et al. CDK19 is disrupted in a female patient with bilateral congenital retinal folds, microcephaly and mild mental retardation. *Hum Genet*. 2010;128:281-291.
24. Castells-Nobau A, Eidhof I, Fenckova M, et al. Conserved regulation of neurodevelopmental processes and behavior by FoxP in Drosophila. *PLoS One*. 2019;14:e0211652.

25. Eidhof I, Baets J, Kamsteeg EJ, et al. GDAP2 mutations implicate susceptibility to cellular stress in a new form of cerebellar ataxia. *Brain*. 2018;141:2592-2604.
26. Synofzik M, Schule R. Overcoming the divide between ataxias and spastic paraplegias: Shared phenotypes, genes, and pathways. *Mov Disord*. 2017;32:332-345.
27. Bindu PS, Taly AB, Sonam K, et al. Bilateral hypertrophic olivary nucleus degeneration on magnetic resonance imaging in children with Leigh and Leigh-like syndrome. *Br J Radiol*. 2014;87:20130478.
28. Hirotsu S, Abe Y, Okada K, et al. Crystal structure of a multifunctional 2-Cys peroxiredoxin heme-binding protein 23 kDa/proliferation-associated gene product. *Proc Natl Acad Sci U S A*. 1999; 96:12333-12338.
29. Li KK, Pang JC, Lau KM, et al. MiR-383 is downregulated in medulloblastoma and targets peroxiredoxin 3 (PRDX3). *Brain Pathol*. 2013;23:413-425.
30. Ishiguro T, Sato N, Ueyama M, et al. Regulatory role of RNA chaperone TDP-43 for RNA misfolding and repeat-associated translation in SCA31. *Neuron*. 2017;94:108-124.e7.
31. Petersen AJ, Katzenberger RJ, Wassarman DA. The innate immune response transcription factor relish is necessary for neurodegeneration in a Drosophila model of ataxia-telangiectasia. *Genetics*. 2013;194:133-142.
32. Altschul SF, Gish W, Miller W, Myers EW, Lipman DJ. Basic local alignment search tool. *J Mol Biol*. 1990;215:403-410.
33. Celniker SE, Dillon LA, Gerstein MB, et al.; modENCODE Consortium. Unlocking the secrets of the genome. *Nature*. 2009; 459:927-930.
34. Robinson SW, Herzyk P, Dow JA, Leader DP. FlyAtlas: Database of gene expression in the tissues of Drosophila melanogaster. *Nucleic Acids Res*. 2013;41:D744-D750.
35. Ismail T, Kim Y, Lee H, Lee DS, Lee HS. Interplay between mitochondrial peroxiredoxins and ROS in cancer development and progression. *Int J Mol Sci*. 2019;20: 4407.
36. Kayashima Y, Yamakawa-Kobayashi K. Involvement of Prx3, a Drosophila ortholog of the thiol-dependent peroxidase PRDX3, in age-dependent oxidative stress resistance. *Biomed Res*. 2012; 33:319-322.
37. Zhang YG, Wang L, Kaifu T, Li J, Li X, Li L. Featured article: Accelerated decline of physical strength in peroxiredoxin-3 knockout mice. *Exp Biol Med (Maywood)*. 2016;241:1395-1400.
38. Wu WB, Menon R, Xu YY, et al. Downregulation of peroxiredoxin-3 by hydrophobic bile acid induces mitochondrial dysfunction and cellular senescence in human trophoblasts. *Sci Rep*. 2016;6:38946.
39. Yun HM, Park KR, Lee HP, et al. PRDX6 promotes lung tumor progression via its GPx and iPLA2 activities. *Free Radic Biol Med*. 2014;69:367-376.
40. Aoyama K, Nakaki T. Impaired glutathione synthesis in neurodegeneration. *Int J Mol Sci*. 2013;14:21021-21044.
41. Piemonte F, Pastore A, Tozzi G, et al. Glutathione in blood of patients with Friedreich's ataxia. *Eur J Clin Invest*. 2001;31: 1007-1011.
42. Tozzi G, Nuccetelli M, Lo Bello M, et al. Antioxidant enzymes in blood of patients with Friedreich's ataxia. *Arch Dis Child*. 2002; 86:376-379.